NANO LETTERS
Cite This: Nano Lett. XXXX, XXX, XXX−XXX
Letter
pubs.acs.org/NanoLett

Ultrathin Polymer Nanofibrils for Solar-Blind Deep Ultraviolet Light Photodetectors Application

Long-Zhen Qiu,[†] Shi-Yu Wei,[†] Hai-Sheng Xu,[‡] Zhi-Xiang Zhang,[§] Zhong-Yi Guo,*[,‡] Xiu-Guo Chen,[∥] Shi-Yuan Liu,[∥] Di Wu,[⊥] and Lin-Bao Luo*[,§]

[†]Academy of Optoelectronic Technology, National Engineering Laboratory of Special Display Technology, [‡]School of Computer and Information, and [§]School of Electronic Science and Applied Physics, Hefei University Technology, Hefei 230009, China
[∥]School of Mechanical Science and Engineering, Huazhong University of Science and Technology, Wuhan 430074, China
[⊥]School of Physics and Microelectronics, Zhengzhou University, Zhengzhou 450052, China

Supporting Information

ABSTRACT: Solar-blind deep ultraviolet photodetectors (DUVPDs) based on conventional inorganic ultrawide bandgap semiconductors (UWBS) have shown promising application in various civil and military fields and yet they can hardly be used in wearable optoelectronic devices and systems for lack of mechanical flexibility. In this study, we report a non-UWBS solar-blind DUVPD by designing ultrathin polymer nanofibrils with a virtual ultrawide bandgap, which was obtained by grafting P3HT with PHA via a polymerization process. Optoelectronic analysis reveals that the P3HT-*b*-PHA nanofibrils are sensitive to DUV light with a wavelength of 254 nm but are virtually blind to both 365 nm and other visible light illuminations. The responsivity is 120 A/W with an external quantum efficiency of up to 49700%, implying a large photoconductive gain in the photoresponse process. The observed solar-blind DUV photoresponse is associated with the resonant mode due to the leakage mode of the ultrathin polymer nanofibrils. Moreover, a flexible image sensor composed of 10 × 10 pixels can also be fabricated to illustrate their capability for image sensing application. These results signify that the present ultrathin P3HT-*b*-PHA nanofibrils are promising building blocks for assembly of low-cost, flexible, and high-performance solar-blind DUVPDs.

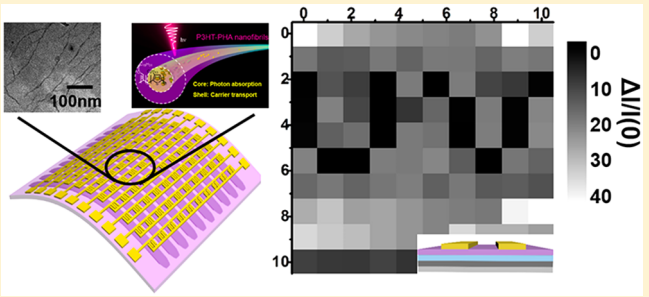

KEYWORDS: *Optoelectronic device, polymer nanostructures, leakage mode, virtual ultrawide bandgap semiconductor, image sensor*

Solar-blind deep ultraviolet photodetector (DUVPD) is a sort of optoelectronic device that can detect photonic irradiation with wavelengths in the range of 200−280 nm.[1,2] As a complement to visible and infrared light (IR) photodetectors (PDs),[3,4] DUVPDs are of paramount importance and have recently received extensive attention for their promising applications in military surveillance, target detection and acquisition, missile launch detection, chemical analysis, and flame detection.[5] For example, DUVPDs have exhibited great potential in biological and medical analysis because DUV photons can be strongly absorbed by DNA molecules, inducing significant damage.[6] In addition, highly responsive solar-blind DUVPDs that are immune to interference from ambient visible or UVA and UVB lights are crucial to track ballistic missile. Therefore, solar-blind DUVPDs have been widely employed in some space-based warning systems.[7]

Benefiting from the rapid advance of semiconductor technology, various high-performance DUVPDs with different device geometries have been developed in the past decades.[8,9] Generally, these devices are made of ultrawide bandgap semiconductors (UWBS), such as Ga_2O_3,[10] $Zn_xMg_{1-x}O$,[11] diamond,[12] and $Al_xGa_{1-x}N$,[13,14] which are normally characterized by a bandgap of around 5 eV or even larger value. Various studies have demonstrated that the UWBS-based DUVPDs can attain excellent DUV sensitivity, including a large on/off ratio, relatively low dark-current, high responsivity, and high rejection ratio.[15] Despite these obvious advantages, these inorganic UWBS DUVPDs have their own shortcomings. For instance, the majority of the above UWBS materials are usually grown by sputtering, plasma-enhanced chemical vapor deposition (PECVD), molecular beam epitaxy (MBE), or even metal−organic chemical vapor deposition (MOCVD), which means the synthesis process is complicated, and the fabrication cost is relatively high.[16] Moreover, the rigid nature of these materials limits their application in flexible and wearable devices.[17,18] From the perspective of mechanical properties, semiconducting polymer materials are suitable for the assembly of flexible optoelectronic devices,[19] which may find applications in wearable medical device and telehome healthcare system. Unfortunately, the majority of conjugate polymer

Received: October 24, 2019
Revised: November 27, 2019
Published: December 2, 2019

Downloaded via HEFEI UNIV OF TECHNOLOGY on December 6, 2019 at 23:37:49 (UTC).
See https://pubs.acs.org/sharingguidelines for options on how to legitimately share published articles.

© XXXX American Chemical Society

DOI: 10.1021/acs.nanolett.9b04410
Nano Lett. XXXX, XXX, XXX−XXX

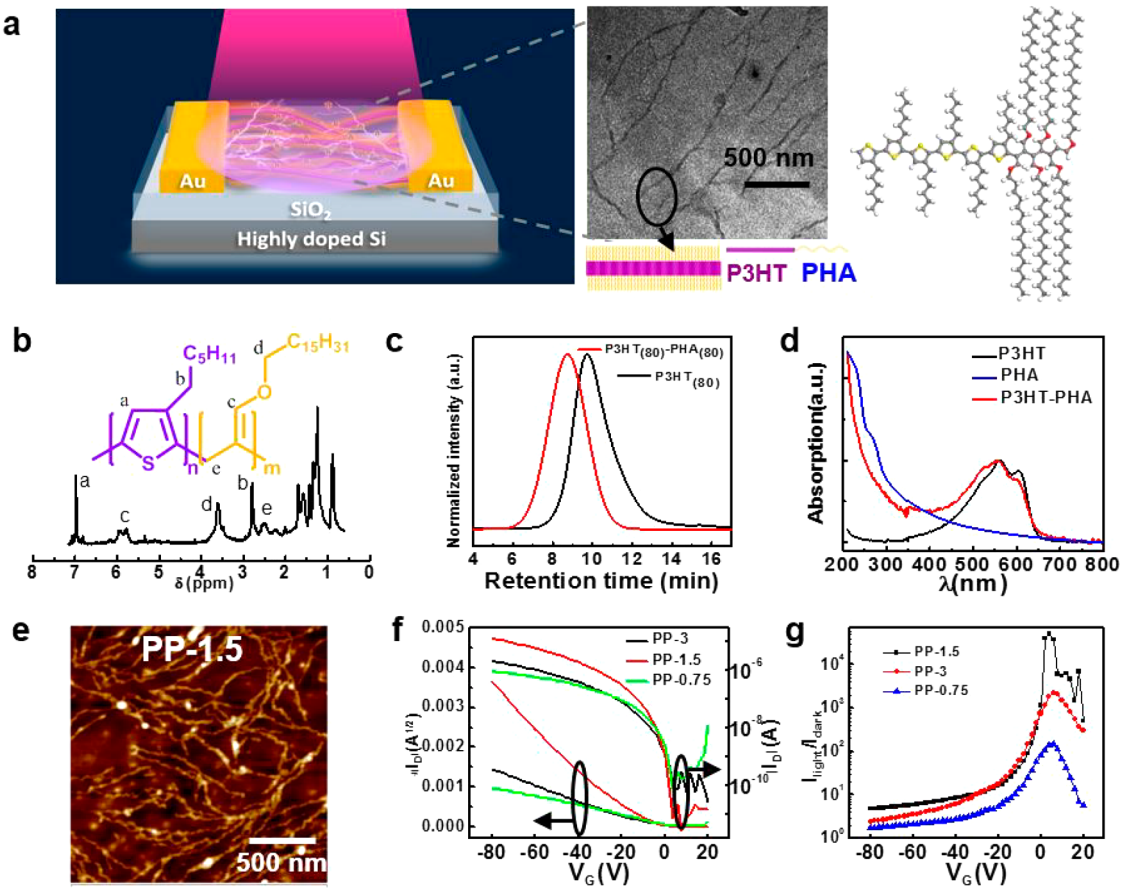

Figure 1. (a) Schematic illustration of P3HT-*b*-PHA nanofibrils FET. (a) TEM image of P3HT-*b*-PHA nanofibrils, the schematic structure of the P3HT-*b*-PHA, and the corresponding molecular structure. (b) ^{1}H NMR spectrum of the P3HT-*b*-PHA. (c) GPC traces of the P3HT-*b*-PHA. (d) Comparison of UV−vis absorption of PHA, P3HT, and P3HT-*b*-PHA films. (e) AFM images of P3HT-*b*-PHA nanofibrils derived from the transfer-etching process. (f) The transfer characteristics of the devices based on PP-0.75, PP-1.5, and PP-3 samples. (g) The photoresponse I_{light}/I_{dark} of the devices PP-0.75, PP-1.5, and PP-3 under 254 nm UV radiation with an intensity of 540 μW/cm^2.

materials have narrow bandgaps, making them more sensitive to visible and near-infrared radiation rather than the DUV region.[20,21]

Here, we report on a highly sensitive a non-UWBS solar-blind DUVPD made of ultrathin poly(3-hexylthiophene)-poly(hexadecyloxyallene) (P3HT-*b*-PHA) nanofibrils with virtual ultrawide bandgap which are synthesized by a simple transfer-etching solution method. Like UWBS, the poly(3-hexylthiophene)-poly(hexadecyloxyallene) (P3HT-*b*-PHA) can absorb DUV light and generate excitons for the selective absorption of shell part (-PHA) in 200−300 nm region. At the same time, the resultant photogenerated carriers can be easily transported by the semiconducting P3HT. Device analysis revealed that the ultrathin P3HT-*b*-PHA nanofibrils were highly sensitive to illumination with a wavelength of 254 nm but were virtually blind to both 365 nm and other illumination in the visible region. Such a solar-blind DUV sensitivity was related to the leakage mode of the ultrathin polymer nanofibrils according to modeling based on finite difference time-domain (FDTD). Furthermore, flexible DUV sensors on a PET substrate with 10 × 10 pixels have been fabricated, and their ability to capture a still DUV image under bending strains has been successfully demonstrated. These results, along with the relatively simple fabrication process, corroborate that the ultrathin P3HT-*b*-PHA nanofibrils are of potential importance in future DUV optoelectronic devices and systems.

Results and Discussion. The device configuration of the nanofibrillar polymer-based DUVPD and the molecular structure are illustrated in Figure 1a. The P3HT-*b*-PHA block copolymer nanofibrils in this study were synthesized through a one-pot sequential polymerization method, as shown in Figure S1 (see SI for detailed information).[22−26] To confirm the chemical structures of the triblock copolymers, ^{1}H nuclear magnetic resonance (NMR) spectroscopy was performed. The ^{1}H NMR data in Figure 1b shows two strong peaks at a (6.98 ppm) and b (2.80 ppm), which can be attributed to the protons of thiophene ring and hexyl side chain of the P3HT block. Moreover, the proton signals at c (5.95, 5.80 ppm), d (3.60 ppm), and e (2.50 ppm) are all due to the group of the PHA block.[23] The characteristic signal of double bond protons of the PHA block at c (5.95, 5.80 ppm) confirms the presence of both cis- and trans-geometries.[23] According to further gel permeation chromatography (GPC) analysis shown in Figure 1c, the number-average molecular weight (Mn) of the as-synthesized homopolymer P3HT$_{(80)}$ and diblock copolymer are determined to be 13.3 and 35.7 kDa, respectively, corresponding to a diblock copolymer structure of P3HT$_{(80)}$-*b*-PHA$_{(80)}$. Figure 1d compares the normalized UV−vis absorption spectra of both P3HT (black line) and P3HT-*b*-PHA (red line) films, from which one can easily find that besides the absorption of P3HT in the 400−600 nm region the P3HT-*b*-PHA shows an extra absorption at 200−300 nm due

DOI: 10.1021/acs.nanolett.9b04410
Nano Lett. XXXX, XXX, XXX−XXX

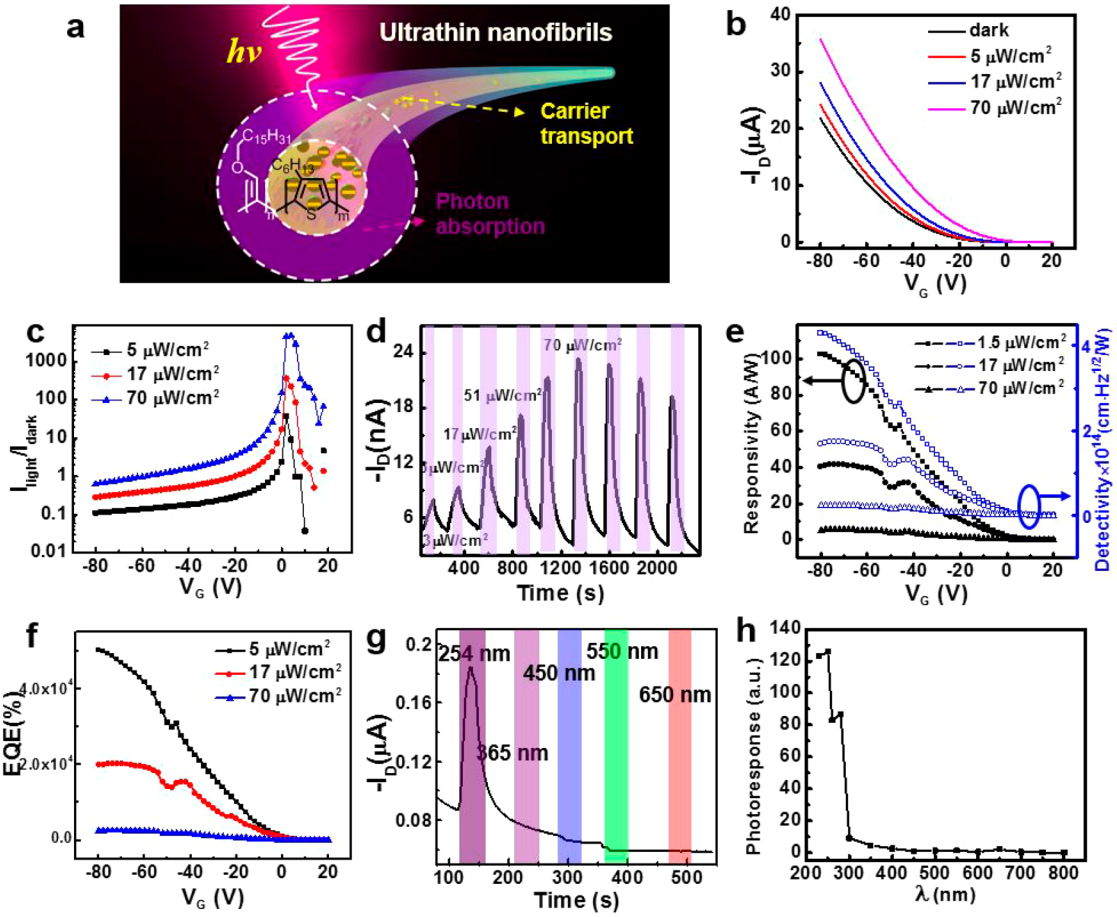

Figure 2. (a) Schematic illustration of the operation mechanism of P3HT-PHA nanofibrils DUVPD under light illumination. (b) Transfer curves of the PP-1.5 in dark and different DUV (254 nm) light intensities. (c) The I_{light}/I_{dark} of the PP-1.5-based device under 254 nm radiation. (d) Time-dependent photoresponse behavior of the DUVPD under light illumination with different intensities. (e) Responsivity and specific detectivity as a function of gate voltage. (f) EQE as a function of gate voltage. (g) The evolution of photocurrent under illumination with different wavelengths. (h) Spectral response of the device based on PP-1.5.

to the characteristic absorption of PHA.[23] Without question, such a strong absorption in the DUV region is highly beneficial for the detection of DUV light illumination. By a transfer-etching method (Figure S2), the P3HT-*b*-PHA material was further transformed to large-scale ultrathin P3HT-*b*-PHA nanofibrils with a diameter of approximately 15 nm, according to the TEM image in Figure 1a.

It should be noted that during the transfer-etching process, the diameter of P3HT-*b*-PHA nanofibrils were kept nearly unchanged, whereas their density was substantially increased when the concentration of P3HT-*b*-PHA in the blending solvent was increased. Figure 1e and Figure S3 show the atomic force microscopy (AFM) images of P3HT-*b*-PHA nanofibrils which were obtained by selecting different concentrations of 0.75, 1.50, and 3.00 mg/mL as precursors. (For convenience, the as-derived samples are labeled as PP-0.75, PP-1.5, and PP-3, respectively.) With increasing P3HT-*b*-PHA concentration, the density of the nanofibrils increases dramatically. Figure S4 illustrates the diameter distribution of the nanofibrils obtained from simulation (Figure S5).[27] The diameters for all three samples are all distributed in the range of 10−20 nm with nearly the same average value. To study the electrical properties of the P3HT-*b*-PHA nanofibrils, organic field effect transistor (OFET) devices with a bottom-gate and top-contact (BGTC) geometry were fabricated. Figure S6 plots the output characteristics of the nanofibril OFETs. The increase in electrical conduction with gate voltage reveals the typical characteristics of the nanofibril OFETs with a p-type channel. By using the linear part of the $I_{ds}-V_g$ curve in Figure 1f, the hole mobilities of all the three devices are calculated and summarized in Table S1. Compared with the other two samples, the P3HT-*b*-PHA device assembled from PP-1.5 exhibits the highest mobility (0.04 $cm^2/(V\ s)$), the smallest subthreshold (SS, 2.24) and lowest threshold voltage (V_{th}, −5.67 V). Notably, when illuminated by DUV light (540 $\mu W/cm^2$) with a wavelength of 254 nm, the three devices all exhibit marked sensitivity (Figure 1g). The I_{light}/I_{dark} (photocurrent/dark current) ratio reaches as high 4.73×10^3 for the PP-1.5 device, representing the highest value in comparison with the other two devices.

The observed sensitivity to DUV illumination can be understood as follows: due to the unique molecular structure, the shell part (-PHA) absorbs the incident DUV light and generate excitons,[23] which drift to the core−shell interface and separate into electrons and holes with the assistance of an external bias,[28] as illustrated by Figure 2a. During this process, the photocurrent is determined by the gate voltage (Figure 2b); when bias voltage changes from 0 to −80 V, the photocurrent increases accordingly. Meanwhile, the I_{light}/I_{dark} ratio increases dramatically due to the sharp decrease in dark

DOI: 10.1021/acs.nanolett.9b04410
Nano Lett. XXXX, XXX, XXX−XXX

Table 1. Comparison of the Key Parameters of the Present Device and Other Devices with Similar Structures

materials and structures	wavelength (nm)	I_{light}/I_{dark} ratio	R [A·W^{-1}]	D^* [cm·Hz$^{1/2}$·W^{-1}]	EQE [%]	reference
P3HT-PHA nanofibrils	254	4000	120	4.2×10^{14}	4.97×10^4	this work
graphene-β-Ga_2O_3	254		39.3	9.9×10^{14}	1.96×10^4	2
β-Ga_2O_3	251		9.7	6.29×10^{12}		10
graphene-microcrystalline diamond	220		1.4	1×10^{13}		30
S-doped diamond	220	5×10^5	10.5			31
ZnMgO	250	10^4	0.00016	1.5×10^{11}		11
ZnO−Ga_2O_3 microwire	254	1.0×10^5	1.3×10^3	9.91×10^{14}	2.92×10^4	15
MoS_2	220		0.004			32
$CsPbX_3$ quantum dots	200		0.054	3.3×10^{14}	22	33

current (Figure 2c). Further photoresponse under different intensities ranging from 3 to 70 μW/cm^2 in Figure 2d reveals that the device can be readily switched between on and off states under different light intensities with good reproducibility between several exposure durations. Moreover, with increasing illumination intensity the photocurrent also increase. It should be noted that when repeatedly illuminating the device with the same light intensity, both the photocurrent and dark current decrease gradually. Such a degradation in photosensitivity is probably due to the instability of OFET device under the bias voltage.[29] Surprisingly, when the illumination wavelength increases, the photoresponse declines sharply and virtually no response is observed when the wavelength is longer than 300 nm (Figure 2e,f). The detailed reason for the blindness to longer wavelengths will be discussed later. Further analysis reveals that the I_{light}/I_{dark} ratio is determined not only by light intensity but also by the applied gate voltage. One can easily observe that when bias voltage changes from 0 to −80 V, the I_{light}/I_{dark} ratio decreases dramatically due to the amplification effect of the gate electrode.

To quantitatively assess the sensitivity of P3HT-*b*-PHA nanofibril DUVPD, both responsivity (R) and specific detectivity (D^*) were calculated. R was estimated using the following equation

$$R = \frac{I_{light} - I_{dark}}{i_p \cdot S} \quad (1)$$

where I_{light} is the current under illumination (24.06 μA), i_p is the light intensity (5 μW/cm^2), I_{dark} is the dark current (23.43 μA), and S is the effective illuminated area (1×10^{-3} cm^2). In addition, the specific detectivity, which is usually used to describe the smallest detectable signal, can be described by the following relationship

$$D^* = \frac{R \cdot S^{1/2}}{(2e \cdot I_{dark})^{1/2}} \quad (2)$$

where e is the electronic charge, which is 1.602×10^{-19} C. On the basis of eq 1, R is estimated to be 120 A/W. I_{dark} and S are the same parameters described above; therefore, D^* is calculated to be 4.2×10^{14} Jones. The external quantum efficiency (EQE), which is defined as the number of electrons probed per incident photon, can be estimated by the following formula

$$EQE = \frac{hcR}{(e\lambda)} \quad (3)$$

where h is Planck's constant (6.626×10^{-34} J·s), c is the velocity of light (3×10^8 m/s), and λ is the exciting wavelength. By using these values, the responsivity, detectivity, and EQE under different intensities are calculated and summarized in Figure 2e, f. It is obvious that when the bias voltage changes from 0 to −80 V, the responsivity, detectivity and EQE increase accordingly. Specifically, at a bias voltage of −80 V these values reach 120 A/W, 4.2×10^{14} cm·Hz$^{1/2}$·W^{-1} and 49700%, respectively. Table 1 compares some key device parameters (e.g., I_{light}/I_{dark}, R, D^*, and EQE) of the present P3HT-PHA nanofibrils (PP-1.5) device and other solar-blind DUVPDs composed of UWBS. It is clear that these parameters are slightly poorer than DUVPDs based on a ZnO−Ga_2O_3 hybrid structure.[15] Nonetheless, they are not only better than DUVPDs composed of graphene-β-Ga_2O_3 heterojunction,[2] β-Ga_2O_3 thin film,[10] graphene-microcrystalline diamond,[30] and S-doped diamond[31] but also than those made of some newer materials such as MoS_2[32] and $CsPbX_3$ quantum dots.[33] Such a relatively good device performance, together with the easy synthesis process, renders our polymer photodetector potentially important for future low-cost optoelectronic devices and systems. One more thing that should be mentioned is that the present ultrathin nanofibril device has a relatively poor ambient stability. The photocurrent will experience a noticeable reduce when exposed in ambient condition without any special treatment. Despite this, we believe the device stability can be retained if any passivation treatment or package work were employed.

The solar-blind DUV light sensitivity of the ultrathin nanofibrils device is completely different from devices assembled from P3HT-b-PHA thin film with a thickness of approximately 80 nm. Figure 3a illustrates the schematic structure of the P3HT-b-PHA thin film device fabricated by a simple spin-coating method, as depicted in Figure S7. Figure S8 shows the output and transfer curves of the P3HT-b-PHA thin film FET. On the basis of the linear part of the $I_{ds}-V_g$ curve, the hole mobility was calculated to be ~10^{-4} cm^2/(V s), four hundred times lower than that of P3HT-b-PHA nanofibrils. This relatively high hole moblity is related to the special synthetic process. When P3HT-b-PHA is mixed with PMMA, the flexible PMMA matrix creates a flexible surrounding environment, which is beneficial for forming a highly ordered molecule stack. This process can greatly facilitate charge transport; therefore, the mobility of P3HT-b-PHA increases dramatically.[34,35] Apart from the huge difference in carrier mobility, the P3HT-b-PHA thin film device also exhibits a different spectral property. The spectral response in Figure 3b,c revealed that in contrast to the P3HT-b-PHA nanofibrils device the thin film PD exhibits broadband sensitivity in the range of 200−800 nm. It exhibits obvious sensitivity not only to 254 nm illumination in the DUV region but also to illumination in UVA and visible light regions. In fact, such a remarkable difference in spectral sensitivity is

DOI: 10.1021/acs.nanolett.9b04410
Nano Lett. XXXX, XXX, XXX−XXX

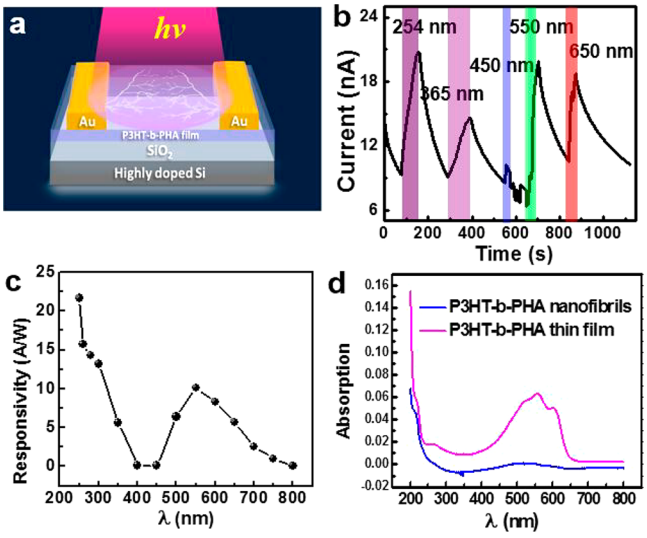

Figure 3. (a) Schematic illustration of the thin film PD. (b) Photoresponse behavior of the 80 nm thin film PD under different light illumination, the gate voltage and drain voltage are kept −80 V and −10 V, respectively. (c) Spectral response of the device made of P3HT-b-PHA thin film. (d) Comparison of the experimental absorption curves of the P3HT-b-PHA thin film and nanofibrils.

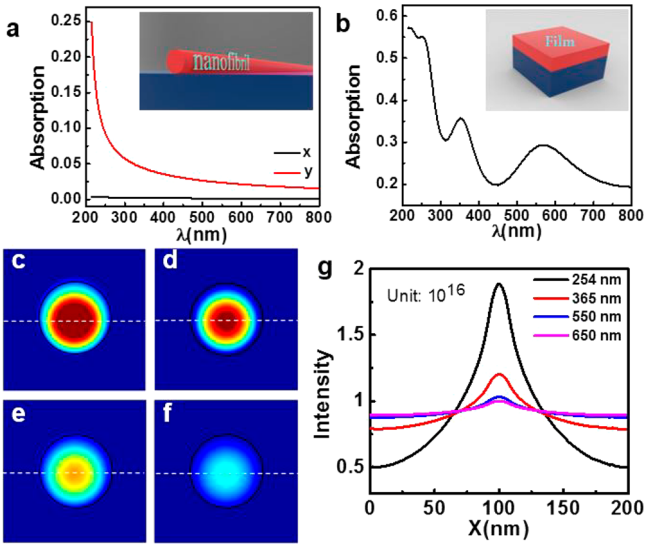

Figure 4. (a) Absorption of P3HT-PHA nanofibril (the inset) under *x*- (black) and *y*-polarized (red) incident light. (b) The absorption of the P3HT-PHA film (the inset) with 80 nm thickness. (c–f) Electric fields of P3HT-PHA nanofibrils in the *x*–*z* plane excited by *y*-polarized incident light with the wavelengths of 254, 365, 550, 650, and 800 nm, respectively. (g) The electric intensities corresponding to dashed lines' positions in (c–f).

consistent with the experimental UV–vis absorption curve in which the P3HT-b-PHA thin film shows strong absorption in both the DUV and 450–650 nm regions, whereas the absorption of P3HT-b-PHA nanofibrils at 450–650 nm is considerably reduced (Figure 3d).

To shed light on the observed difference in photoresponse, the optical properties of both P3HT-PHA nanofibrils and thin film were theoretically simulated and compared using FDTD method. (The optical constant of P3HT-PHA was obtained from the experiment, which is provided in Figure S9.) In the simulations, the diameter of the P3HT-PHA nanofibrils is 15 nm, and the thickness of P3HT-PHA thin film is set to be 80 nm. The P3HT-PHA film can absorb light not only in DUV region but also in the visible and UVA regions (Figure 4b). Further simulation finds that the P3HT-PHA nanofibrils only absorb DUV light. Specifically, the absorption characteristic is highly dependent on the incident polarizations. The nanofibrils can hardly absorb *x*-polarized light but they can absorb *y*-polarized light in the DUV region (Figure 4a). This difference between the two structures originates from the resonance between the one-dimensional nanostructure and polarized light.[36] To further investigate the physical mechanism and the absorption difference of the P3HT-PHA nanofibrils in both visible and ultraviolet bands, the electric fields of the nanofibrils at the wavelengths of 254, 365, 550, and 650 nm under *y*-polarization incidence are extracted and shown in Figure 4c–f, respectively. It is obvious that under 254 nm illumination, the incident electric field can be trapped along the nanofibrils efficiently by exciting the TM01 resonant mode due to the leakage mode.[37] However, with increasing incident wavelength (Figure 4c–f), the intensities of the trapped electric fields in the nanofibrils decreases, as depicted in Figure 4g. In fact, this evolution in the electric field of the resonant mode is understandable considering that with the increase of incident wavelength, the excited capacity of the resonant mode (TM01) due to the leakage mode will be reduced (for a nanofibril with a diameter of 15 nm, its cutoff wavelength is only 118 nm. Therefore, only the TM01 mode exists under illuminations of 254, 365, 550, and 650 nm). In fact, similar phenomenon was also observed in other ultrathin nanofibrials with diameters of 10 and 6 nm (Figure S10).

The ability to record image information with high resolution is of paramount importance in commercial imaging devices, such as cameras, fax machines, and so forth. To explore the possible application of P3HT-b-PHA nanofibril-based solar-blind DUVPD, a flexible image sensor with 10 × 10 pixels was fabricated (Figure 5a). During device fabrication, 30 nm thick aluminum strips were evaporated onto the plastic substrate poly(ethylene terephthalate) (PET) to serve as gate electrodes, and perfluoro(1-butenyl vinyl ether) polymer (CYTOP) was spin-coated as the dielectric layer. PHA-1.5 nanofibrils were then formed by the process above, followed by the deposition of source/drain electrodes. All pixels on the PET substrate show pronounced sensitivity to 254 nm illumination. Figure 5b shows the representative source-drain current as a function of bias voltage, from which one can see that the photocurrent of the PP-1.5 nanofibrils device increase gradually when the light intensity increases from 17 to 540 μW/cm^2. Figure 5c shows the image produced by projecting a "UV" optical pattern onto the P3HT-b-PHA nanofibrils PD array without bending, collecting, and displaying the photocurrent distribution in the computer. It is obvious that the character "UV" was successfully projected onto the nanofibrils image sensor. As a matter of fact, the image was still clear even when the device was bent at an angle of 5° (Figure 5d). Nonetheless, when choosing either 365 nm or white light as projection light, no obvious "UV" projection was obtained (Figure 5e,f). This result confirms that the present P3HT-b-PHA nanofibril PD array can be used for solar-blind DUV imaging applications.

In summary, a non-UWBS solar blind DUV phototransistor was developed based on ultrathin P3HT-b-PHA nanofibrils with virtual ultrawide bandgap which is characterized by a shell part (-PHA) that can absorb DUV light and generate excitons,

DOI: 10.1021/acs.nanolett.9b04410
Nano Lett. XXXX, XXX, XXX–XXX

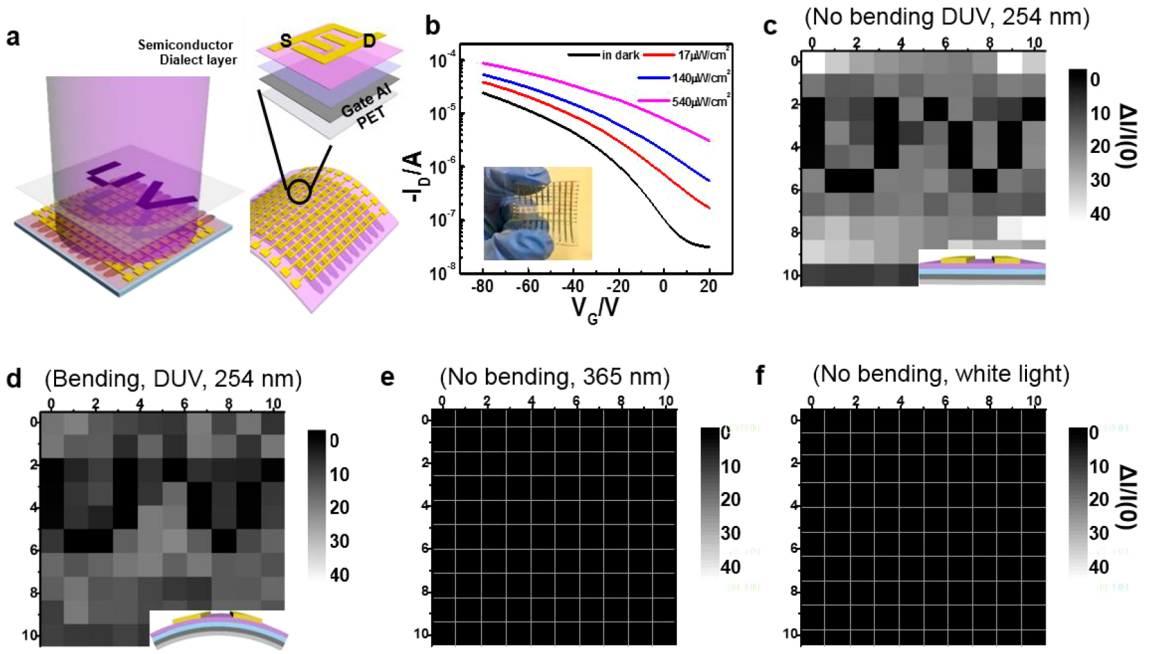

Figure 5. (a) Schematic illustration of the obtained image sensor array and photographic image of this device upon bending. (b) Transfer-curve of a single device in the array under different DUV light intensities; the inset shows the schematic of the image sensor array partially masked and exposed to DUV (254 nm). (c) Image sensing mapping of the image sensor matrix tested in flat (c) and bending conditions under DUV (d), 365 nm (e), and 150 mW/cm^2 white light illumination (f).

and the shell part (-P3HT) that is beneficial for charge transport. The polymer nanofibrils derived by a simple transfer-etching method have an average diameter of approximately 15 nm, with a hole mobility as high as 0.04 $cm^2V^{-1}s^{-1}$. A PD based on the P3HT-b-PHA nanofibrils exhibits excellent solar-blind sensitivity; it is highly sensitive to 254 nm illumination with a responsivity of 120 A/W but is nearly blind to illumination from 365 nm to the visible light region. This spectral response is associated with the leakage mode of the ultrathin polymer nanofibrils according to FDTD simulation. Flexible DUV sensors on a PET substrate with 100 pixels have been fabricated, and their ability to capture a still DUV image under bending strain have been successfully demonstrated. The totality of the above study suggests that the present solution-processed polymer nanofibrils are ideal building blocks for the assembly of highly sensitive and flexible DUVPDs, which may find potential applications in future low-cost wearable optoelectronic devices and systems.

Experimental Section. *Materials Synthesis and Characterization.* Poly(methyl methacrylate) (PMMA) (Mw ~ 996 kDa) and chlorobenzene (CB) were purchased from Sigma-Aldrich. The CYTOP was purchased from AGC Asahi Glass. In this study, P3HT-b-PHA was synthesized by a one-pot sequential polymerization, which has been reported previously.[23−26] To prepare the P3HT-b-PHA nanofibrils, P3HT-b-PHA and PMMA were separately dissolved in chlorobenzene and dichlorobenzene, respectively, and mixed at optimum concentrations of P3HT-b-PHA (0.75, 1.50, and 3.00 mg/mL) and PMMA (3 wt %). The mixed solutions were then spin-coated onto clean silicon substrates at 2000 rpm for 60 s in a glovebox. After drying overnight in a vacuum oven to remove the solvent, the silicon wafer samples were immersed in deionized water to strip the thin film from the silicon surface. The as-obtained films were rinsed in deionized water and transferred to SiO_2/Si substrates or PET substrates, and finally transitioned to P3HT-b-PHA nanofibrils by rinsing with ethyl acetate to remove the PMMA matrix. The morphologies and the thickness of the polymer thin films were investigated using tapping-mode atomic force microscopy (AFM) (Nanoscope, Veeco Instrument Inc.). Field-emission transmission electron microscopy (TEM) observations were conducted on a high-resolution JEM-2100F field-emission transmission electron microscope. The samples for TEM characterization were obtained by peeling off the spin-cast films on silica substrates and subsequently transferring those onto 200 mesh copper grids. The UV−vis spectroscopy (UV−vis) measurements were performed on a UNIC 4802 UV/vis double beam spectrophotometer.

Device Fabrication and Analysis. In the study, two kinds of device geometries were fabricated and investigated. The first device geometry is a bottom-gate P3HT-b-PHA nanofibril transistor on SiO_2/Si, in which the source and drain were fabricated by thermally evaporating a 30 nm thick gold electrode with the assistance of a shadow mask (the channel width is approximately 100 μm). To construct the flexible bottom-gate P3HT-b-PHA nanofibrils' transistor, ribbon-like Al electrodes were first evaporated on a PET substrate to serve as gate electrodes. CYTOP solvent was then spin-coated on the gate electrodes as the dielectric layer onto which a film of P3HT-b-PHA nanofibrils was then transferred by the above solution approach. Finally, the source−drain electrode arrays were deposited on the nanofibrils by a second thermal evaporation. The FET electrical characteristics were measured by a Keithley 4200-SCS instrument in the ambient atmosphere. The field-effect mobility of the devices was obtained in the saturation regime from the highest slope of the $|I_D|^{1/2}$ versus V_G plots by using eq 4

$$I_D = \frac{WC_i}{2L}\mu(V_G - V_T)^2 \quad (4)$$

DOI: 10.1021/acs.nanolett.9b04410
Nano Lett. XXXX, XXX, XXX−XXX

where I_D is the drain−source current, V_G is the gate voltage, V_D is the drain−source voltage, C_i is the capacitance per unit area, and L and W are the channel length and width, respectively. The optoelectronic properties of the solar-blind DUVPD were studied by a Keithley 4200-SCS instrument equipped with a monochromatic LED light source, from which the incident DUV light was directly focused and guided onto the device. Prior to device analysis, the power intensity of the incident light was calibrated by a power meter (Thorlabs GmbH., PM 100D). Unless otherwise specified, all the measurements were carried out at room temperature.

Numerical Simulation. All numerical simulations were performed using the custom-programmed FDTD algorithm. In the calculations, the plane wave propagated along the z-axis with a power of 1 W, and the wavelength range was set in the range of 215−800 nm. Periodic boundary conditions were set in the x- and y-directions of the unit structure to simulate an infinite number of nanowire structures and an infinite length of nanowires in the simulations. Meanwhile, the 400 nm thickness of the perfectly matching layer was set at the top and bottom of the structure to avoid nonphysical reflections of outgoing electromagnetic waves. The absorption value was obtained based on the sum of the incident power minus transmitted and reflected power under the principle of energy conservation. In addition, the air permittivity was 1 in all simulations.

■ ASSOCIATED CONTENT

Supporting Information

The Supporting Information is available free of charge at https://pubs.acs.org/doi/10.1021/acs.nanolett.9b04410.

Additional information, figures, and table (PDF)

■ AUTHOR INFORMATION

Corresponding Authors

*E-mail: guozhongyi@hfut.edu.cn.
*E-mail: luolb@hfut.edu.cn.

ORCID

Long-Zhen Qiu: 0000-0002-8356-6303
Zhong-Yi Guo: 0000-0001-7282-2503
Xiu-Guo Chen: 0000-0002-7067-5084
Shi-Yuan Liu: 0000-0002-0756-1439
Di Wu: 0000-0003-3266-0612
Lin-Bao Luo: 0000-0001-8651-8764

Notes

The authors declare no competing financial interest.

■ ACKNOWLEDGMENTS

The authors thanks Prof. Hoe Hark Tan from Australia National University and Prof. Yuan-Yuan Zhu from Hefei University of Technology for their helpful discussion and constructive comments on this work. This work was supported by the National Natural Science Foundation of China (NSFC, Nos. 51573036, 61675062, 61775050, and 51525502), the Distinguished Youth Foundation of Anhui Province (1808085J03), the Fundamental Research Funds for the Central Universities (JZ2018HGPB0275, JZ2018HGPB0276, JZ2018HGXC0001, and JZ2018HGTA0220), and the Open Foundation of Anhui Provincial Key Laboratory of Advanced Functional Materials and Devices (4500-411104/011).

■ REFERENCES

(1) Oshima, T.; Okuno, T.; Arai, N.; Suzuki, N.; Ohira, S.; Fujita, S. Vertical Solar-Blind Deep-Ultraviolet Schottky Photodetectors Based on β-Ga_2O_3 Substrates. *Appl. Phys. Express* **2008**, *1*, 011202.

(2) Kong, W. Y.; Wu, G. A.; Wang, K. Y.; Zhang, T. F.; Zou, Y. F.; Wang, D. D.; Luo, L. B. Graphene-β-Ga_2O_3 Heterojunction for Highly Sensitive Deep UV Photodetector Application. *Adv. Mater.* **2016**, *28*, 10725−10731.

(3) McDonald, S. A.; Konstantatos, G.; Zhang, S. G.; Cyr, P. W.; Klem, E. J. D.; Levina, L.; Sargent, E. H. Solution-Processed PbS Quantum Dot Infrared Photodetectors and Photovoltaics. *Nat. Mater.* **2005**, *4*, 138−142.

(4) Fu, L.; Lever, R.; Sears, K.; Tan, H. H.; Jagadish, C. $In_{0.5}Ga_{0.5}As$/GaAs Quantum Dot Infrared Photodetectors Grown by Metal-Organic Chemical Vapor Deposition. *IEEE Electron Device Lett.* **2005**, *26*, 628−630.

(5) Pearton, S. J.; Norton, D. P.; Ren, F. The Promise and Perils of Wide-Bandgap Semiconductor Nanowires for Sensing, Electronic, and Photonic Applications. *Small* **2007**, *3*, 1144−1150.

(6) Kapp, F. G.; Perlin, J. R.; Hagedorn, E. J.; Gansner, J. M.; Schwarz, D. E.; O'Connell, L. A.; Johnson, N. S.; Amemiya, C.; Fisher, D. E.; Wolfle, U. Protection from UV light is an Evolutionarily Conserved Feature of the Taematopoietic Niche. *Nature* **2018**, *558*, 445−448.

(7) Keppler, F.; Vigano, I.; McLeod, A.; Ott, U.; Fruchtl, M.; Rockmann, T. Ultraviolet-Radiation-Induced Methane Emissions From Meteorites and the Martian Atmosphere. *Nature* **2012**, *486*, 93−96.

(8) Razeghi, M. Short-Wavelength Solar-Blind Detectors—Status, Prospects, and Markets. *Proc. IEEE* **2002**, *90*, 1006−1014.

(9) Lu, Y. J.; Lin, C. N.; Shan, C. X. Optoelectronic Diamond: Growth, Properties, and Photodetection Applications. *Adv. Opt. Mater.* **2018**, *6*, 1800359.

(10) Oshima, T.; Okuno, T.; Fujita, S. β-$Al_{2x}Ga_{2-2x}O_3$ Thin Film Growth by Molecular Beam Epitaxy. *Jpn. J. Appl. Phys.* **2007**, *46*, 7217−7220.

(11) Fan, M. M.; Liu, K. W.; Zhang, Z. Z.; Li, B. H.; Chen, X.; Zhao, D. X.; Shan, C. X.; Shen, D. Z. High-Performance Solar-Blind Ultraviolet Photodetector Based on Mixed-Phase ZnMgO Thin Film. *Appl. Phys. Lett.* **2014**, *105*, 011117.

(12) Whitfield, M. D.; Chan, S. S.; Jackman, R. B. Thin Film Diamond Photodiode for Ultraviolet Light Detection. *Appl. Phys. Lett.* **1996**, *68*, 290−292.

(13) Brendel, M.; Helbling, M.; Knigge, A.; Brunner, F.; Weyers, M. Measurement and Simulation of Top- and Bottom-Illuminated Solar-Blind AlGaN Metal-Semiconductor-Metal Photodetectors with High External Quantum Efficiencies. *J. Appl. Phys.* **2015**, *118*, 244504.

(14) Mazzeo, G.; Conte, G.; Reverchon, J. L.; Dussaigne, A.; Duboz, J. Y. Deep Ultraviolet Detection Dynamics of AlGaN Based Devices. *Appl. Phys. Lett.* **2006**, *89*, 223513.

(15) Zhao, B.; Wang, F.; Chen, H.; Wang, Y.; Jiang, M.; Fang, X.; Zhao, D. Solar-Blind Avalanche Photodetector Based on Single ZnO-Ga_2O_3 Core-Shell Microwire. *Nano Lett.* **2015**, *15*, 3988−3993.

(16) Xie, C.; Lu, X. T.; Tong, X. W.; Zhang, Z. X.; Liang, F. X.; Liang, L.; Luo, L. B.; Wu, Y. C. Recent Progress in Solar-Blind Deep-Ultraviolet Photodetectors Based on Inorganic Ultrawide Bandgap Semiconductors. *Adv. Funct. Mater.* **2019**, *29*, 1806006.

(17) Sun, Y.; Choi, W. M.; Jiang, H.; Huang, Y. Y.; Rogers, J. A. Controlled buckling of semiconductor nanoribbons for stretchable electronics. *Nat. Nanotechnol.* **2006**, *1*, 201−207.

(18) Lee, S.; Nathan, A. Subthreshold Schottky-barrier thin-film transistors with ultralow power and high intrinsic gain. *Science* **2016**, *354*, 302−304.

(19) Root, S. E.; Savagatrup, S.; Printz, A. D.; Rodriquez, D.; Lipomi, D. J. Mechanical Properties of Organic Semiconductors for Stretchable, Highly Flexible, and Mechanically Robust Electronics. *Chem. Rev.* **2017**, *117*, 6467−6499.

DOI: 10.1021/acs.nanolett.9b04410
Nano Lett. XXXX, XXX, XXX−XXX

(20) O'Brien, G. A.; Quinn, A. J.; Tanner, D. A.; Redmond, G. A. A Single Polymer Nanowire Photodetector. *Adv. Mater.* **2006**, *18*, 2379−2383.
(21) Armin, A.; Jansen-van Vuuren, R. D.; Kopidakis, N.; Burn, P. L.; Meredith, P. Narrowband Light Detection via Internal Quantum Efficiency Manipulation of Organic Photodiodes. *Nat. Commun.* **2015**, *6*, 6364.
(22) Ge, F.; Wei, S.; Liu, Z.; Wang, G.; Wang, X.; Zhang, G.; Lu, H.; Cho, K.; Qiu, L. Z. Bar-Coated Ultrathin Semiconductors from Polymer Blend for One-Step Organic Field-Effect Transistors. *ACS Appl. Mater. Interfaces* **2018**, *10*, 9602−9611.
(23) Yu, Z. P.; Ma, C. H.; Wang, Q.; Liu, N.; Yin, J.; Wu, Z. Q. Polyallene-block-polythiophene-block-polyallene Copolymers: One-Pot Synthesis, Helical Assembly, and Multiresponsiveness. *Macromolecules* **2016**, *49*, 1180−1190.
(24) Wu, Z. Q.; Chen, Y.; Wang, Y.; He, X. Y.; Ding, Y. S.; Liu, Na. One Pot Synthesis of Poly(3-hexylthiophene)-Block-Poly-(hexadecyloxylallene) by Sequential Monomer Addition *Chem. Chem. Commun.* **2013**, *49*, 8069−8071.
(25) Hu, Y. Y.; Su, M.; Ma, C. H.; Yu, Z.; Liu, N.; Yin, J.; Ding, Y.; Wu, Z. Q. Multiple Stimuli-Responsive and White-Light Emission of One-Pot Synthesized Block Copolymers Containing Poly(3-hexylthiophene) and Poly(triethyl glycol allene) Segments. *Macromolecules* **2015**, *48*, 5204−5212.
(26) Yu, Z. P.; Liu, N.; Yang, L.; Jiang, Z. Q.; Wu, Z. Q. One-Pot Synthesis, Stimuli Responsiveness, and White-Light Emissions of Sequence-Defined ABC Triblock Copolymers Containing Polythiophene, Polyallene, and Poly(phenyl isocyanide) Blocks. *Macromolecules* **2017**, *50*, 3204−3214.
(27) Persson, N. E.; McBride, M. A.; Grover, M. A.; Reichmanis, E. Automated Analysis of Orientational Order in Images of Fibrillar Materials. *Chem. Mater.* **2017**, *29*, 3−14.
(28) Kim, Y.; Kim, H. J.; Kim, J. S.; Yun, H.; Park, H.; Han, J.; Kim, B. J. Modulating Regioregularity of Poly(3-hexylthiophene)-based Amphiphilic Block Copolymers To Control Solution Assembly from Nanowires to Micelles. *Chem. Mater.* **2018**, *30*, 7912−7921.
(29) Lee, W. H.; Choi, H. H.; Kim, D. H.; Cho, K. Microstructure Dependent Bias Stability of Organic Transistors. *Adv. Mater.* **2014**, *26*, 1660−1680.
(30) Wei, M.; Yao, K.; Liu, Y.; Yang, C.; Zang, X.; Lin, L. A. A Solar-Blind UV Detector Based on Graphene-Microcrystalline Diamond Heterojunctions. *Small* **2017**, *13*, 1701328.
(31) Mendoza, F.; Makarov, V.; Weiner, B. R.; Morell, G. Solar-Blind Field-Emission Diamond Ultraviolet Detector. *Appl. Phys. Lett.* **2015**, *107*, 201605.
(32) Khan, M. F.; Iqbal, M. W.; Iqbal, M. Z.; Shehzad, M. A.; Seo, Y.; Eom, J. Photocurrent Response of MoS_2 Field-Effect Transistor by Deep Ultraviolet Light in Atmospheric and N_2 Gas Environments. *ACS Appl. Mater. Interfaces* **2014**, *6*, 21645−21651.
(33) Lu, J.; Sheng, X.; Tong, G.; Yu, Z.; Sun, X.; Yu, L.; Xu, X.; Wang, J.; Xu, J.; Shi, Y.; Chen, K. Ultrafast Solar-Blind Ultraviolet Detection by Inorganic Perovskite $CsPbX_3$ Quantum Dots Radial Junction Architecture. *Adv. Mater.* **2017**, *29*, 1700400.
(34) Yu, K.; Park, B.; Kim, G.; Kim, C. H.; Park, S.; Kim, J.; Jung, S.; Jeong, S.; Kwon, S.; Kang, H.; Kim, J.; Yoon, M. H.; Lee, K. Optically Transparent Semiconducting Polymer Nanonetwork for Flexible and Transparent Electronics (SI) *P. Proc. Natl. Acad. Sci. U. S. A.* **2016**, *113*, 14261−14266.
(35) Wang, S.; Fabiano, S.; Himmelberger, S.; Puzinas, S.; Crispin, X.; Salleo, A.; Berggren, M. Experimental Evidence that Short-Range Intermolecular Aggregation is Sufficient for Efficient Charge Transport in Conjugated Polymers. *Proc. Natl. Acad. Sci. U. S. A.* **2015**, *112*, 10599−10604.
(36) Nichol, J. M.; Hemesath, E. R.; Lauhon, L. J.; Budakian, R. Displacement Detection of Silicon Nanowires by Polarization-Enhanced Fiber-Optic Interferometry. *Appl. Phys. Lett.* **2008**, *93*, 193110.
(37) Cao, L. Y.; White, J. S.; Park, J. S.; Schuller, J. A.; Clemens, B. M.; Brongersma, M. L. Engineering Light Absorption in Semiconductor Nanowire Devices. *Nat. Mater.* **2009**, *8*, 643−647.

DOI: 10.1021/acs.nanolett.9b04410
Nano Lett. XXXX, XXX, XXX−XXX